Advances in Ultrafast Optics and Imaging Applications

Guy Satat[a], Barmak Heshmat[a], Nikhil Naik[a], Albert Redo-Sanchez[a], and Ramesh Raskar[a]

[a]Media Lab, Massachusetts Institute of Technology, Cambridge MA, USA

ABSTRACT

Ultrafast imaging has been a key enabler to many novel imaging modalities, including looking behind corners and imaging behind scattering layers. With picosecond time resolution and unconventional sensing geometries, ultrafast imaging can fundamentally impact sensing capabilities in industrial and biomedical applications. This paper reviews the fundamentals, recent advances, and the future prospects of ultrafast imaging-based modalities.

Keywords: Ultrafast Imaging, Computational Imaging

1. INTRODUCTION

The use of ultrafast imaging has been a fundamental piece to many advances in various imaging applications, including looking behind corners,[1] imaging behind scattering layers[2–4] and pose estimation.[5] Critical components to these advances are emerging image sensors with picosecond (ps) time resolution, which enable accurate temporal information acquisition without the need for conventional interferometric geometries.[6] Typical computational imaging techniques in traditional scene analysis exploit sensor parameters such as spatial resolution,[7] angular sensitivity,[8] wavelength, and polarization.[9] However, these parameters alone are limited in their ability to capture the complex dynamics of light propagation. Ultrafast time-resolved sensors overcome this limitation and enable complicated analysis of light-in-flight in various imaging geometries.

One of the most notable applications of ultrafast optics is imaging beyond the conventional field of view of the camera. The sensor measures the time of flight (ToF) of indirect reflections from the hidden object, and a reconstruction algorithm is used to invert the measurements to recover the object. Based on the Plenoptic function,[10] light transport theory[11] and the rendering equation,[12] it has been shown that time-resolved imaging is especially suited for these applications.[13]

To use ultrafast measurements for sensing beyond line-of-sight or conventional field of view, we usually need to solve a complex inverse problem. A key insight in solving the inverse problem is to treat light propagation between the scene and sensors in a five dimensional space[14] comprising of space (2D), angle (2D), and time (1D). Thus, by combining forward models of light propagation and advanced signal processing and optimization techniques, we are able to invert the measurement and recover the hidden scene.

In this paper we demonstrate how ultrafast imaging has enabled simultaneous localization and identification of objects with temporal signatures hidden behind scattering layers. The paper is structured as follows: Section 2 serves as an introduction to ultrafast optical measurement techniques. Section 3 discusses non-line of sight imaging in cases of discrete scattering events. Section 4 discusses non-line of sight imaging in cases where the time dependency is a continuous function. Section 5 extends the discussion to the THz regime. Section 6 discusses novel imaging architectures, and section 7 provides an insight to future ultrafast sensors and their imaging applications.

2. IMAGING WITH ULTRAFAST OPTICS

A key component to ultrafast imaging is the ultrafast sensor. There is a broad range of sensors and sensor arrays that can be used for time-resolved imaging with temporal resolution as low as the ultrafast pulse cycle itself.[15–17] Despite the large diversity of sensors for this application, electronically-triggered sensors, such as streak camera and single photon avalanche diode arrays (SPADs), are more common due to convenience in alignment and

Corresponding author email: guysatat@mit.edu

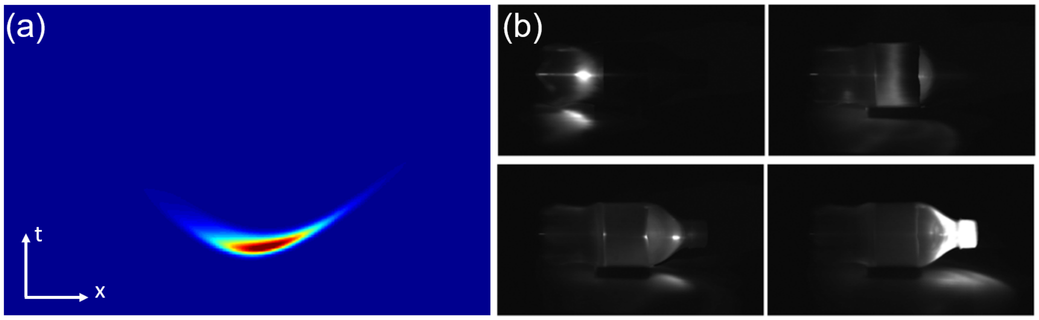

Figure 1. Measurement and result of ultrafast imaging. (a) Streak image, y-axis represents time, x-axis represents spatial coordinates. The target is a patch behind a thin diffuser. Each row represent a time window of $2ps$. (b) Four frames from an ultrafast measurement. The target is a pulse of light propagating through a bottle. Measurements were taken using a streak camera and mechanical moving mirrors (scanning through the spatial y-axis).

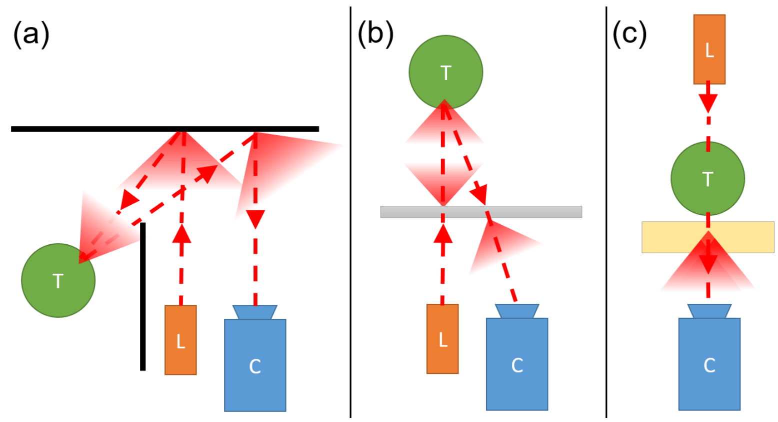

Figure 2. Acquisition geometries for non-line of sight imaging using ultrafast optics. 'T' represents the target. 'C' represents the camera (sensor), and 'L' represents the pulsed laser source. (a) Looking behind corner setup. Black lines are opaque diffusive walls. (b) Imaging through diffuser, reflection mode. Gray line is a thin diffusive sheet. (c) Imaging through diffuser, transmission mode. Yellow box is a volumetric diffuser.

acquisition. The use of electronic triggering through photodiode signal eliminates the need for precise optical delay lines and interferometric geometries.

Streak cameras are photocathode tubes that map the time axis onto the y-axis of a sensor (with $2ps$ time resolution). This is achieved by deflecting photoexcited electrons inside the photocathode tube. The streak image is thus an $x - t$ image (Fig. 1a). In order to acquire the full $x - y - t$ data cube, vertical scanning of the scene is needed. This can be done in a single shot by optical multiplexing[18,19] or it can be done in periodic mode through mechanical scanning means. An example of an ultrafast scene captured with a streak camera and mechanical scanning of the y-axis is shown in Fig. 1b.[20] Full $x - y - t$ scanning is not always necessary. Depending on the application, illumination scanning may replace the vertical scanning. This is known as dual photography[21] and will be demonstrated in multiple applications below.

Streak camera is especially proper for non-line of sight acquisition geometries as it provides nanosecond (ns) time window along with ps time resolution and $\sim 1K$ pixels for spatial resolution. This is not the case for some other electronically triggered ultrafast sensors such as ICCDs[22–24] and SPADs. Another aspect to consider is spectral sensitivity. The majority of the above sensors is broadband; however, since they are mostly based on direct band gap photoexcitation in semiconductors, they lose their sensitivity in far IR and THz.[25] For these frequencies, nonlinear optoelectronic approaches are paving the way for ultrafast imaging.[26,27]

Fig. 2 reviews three main geometries that use ultrafast measurement for non-line of sight imaging. As explained in the following sections, each geometry is better suited for imaging through a certain type of scattering barriers. For example, reflective geometries allow imaging through discrete scattering barriers (Fig. 2a,b). Transmission geometries (Fig. 2c) are desired in case of volumetric scattering for improved signal-to-noise ratio (SNR).

3. IMAGING AFTER DISCRETE SCATTERING EVENTS

3.1 Looking Around Corners

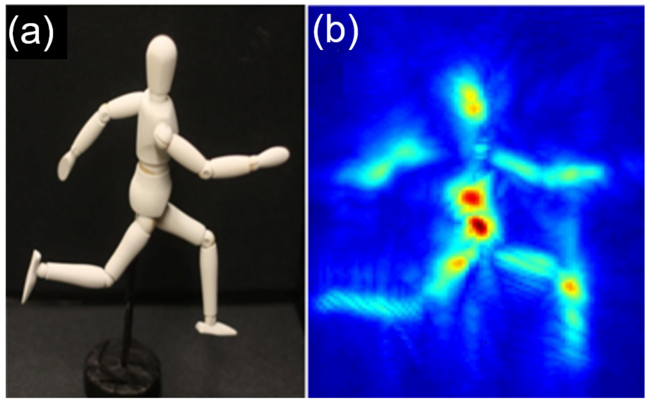

Figure 3. Recovered geometry of hidden object. a) A photograph of a hidden mannequin. b) The recovered geometry using ultrafast time-resolved measurement.

Consider an optical geometry of looking around a corner (Fig. 2a). Using ultrafast time-resolved measurement allows us to recover a mannequin (Fig. 3) hidden behind the corner.[1,28] This is achieved by illuminating the first surface in front of the camera (a door) by a short laser pulse ($\sim 50fs$). The pulse bounces off the door and scatters in all directions. A small fraction of the light will travel into the room, scatter from the hidden object there and travel back, first to the door, and then to the camera. To increase the measurement diversity, it is repeated 60 times, each measurement taken with a different illumination position on the door (using the concept of dual photography[21]).

To reconstruct the hidden object using the ultrafast measurements, we first develop a mathematical model which describes the image formation. Consider a hidden patch in position x', and illumination point on the wall x_l. The captured time-resolved measurement at sensor position x and time t will be:

$$I_l(x,t) = I_0 \int g(x_l, x, x') R(x') \underset{t}{*} \delta\left(t - c^{-1}(r_l(x') + r_c(x'))\right) dx' \tag{1}$$

where, I_0 is the source intensity, and $g(x_l, x, x')$ is a geometric factor which accounts for scene geometry. $R(x')$ is the reflectance of the patch. The $\delta(\cdot)$ function enforces the information cone defined by the speed of light c. Finally, r_l and r_c are the distances from the source to the patch and patch to camera, respectively. The goal is to recover the reflectance distribution $R(x')$ from the set of ultrafast measurements $\{I_l(x,t)\}_{l=1..60}$.

Using this forward model allows to scan through the target volume (x') and compare the expected measurement to the actual measurement. The amount of overlap provides a confidence measure to the existence of object in that location. Repeating this process on the target volume and for all illumination points results in the reconstruction in Fig. 3b.

3.2 Recovering Material Reflectances Behind Scattering Layer

Measuring the reflectance properties of materials—in the form of simple albedo or diffuse reflectivity (as discussed earlier), or complex Bidirectional Reflectance Distribution Functions—is useful for a variety of applications in Optics, Medical Imaging, and Computer Graphics. To demonstrate accurate recovery of these material properties behind scattering layer,[2,29,30] we employ the reflection optical geometry (Fig. 2b).

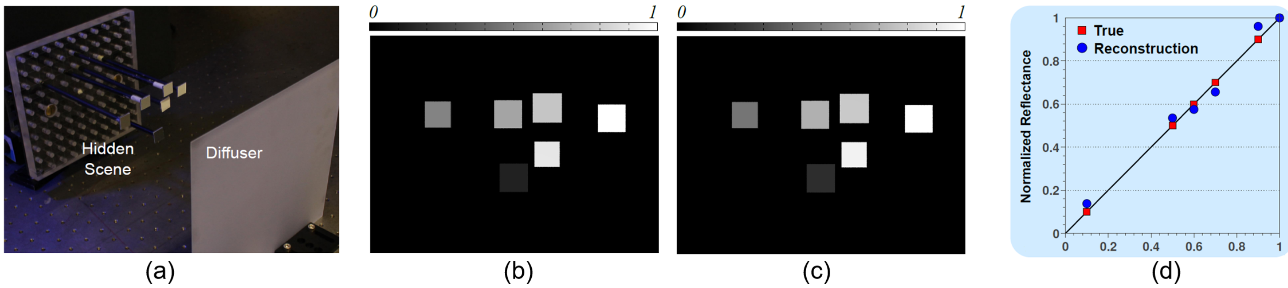

Figure 4. Recovering albedo behind diffuser. (a) Diffuser and hidden scene composed of multiple patches with different albedos. (b) Ground truth albedos. (c) Recovered albedos. (d) Quantitative comparison of recovery to ground truth.

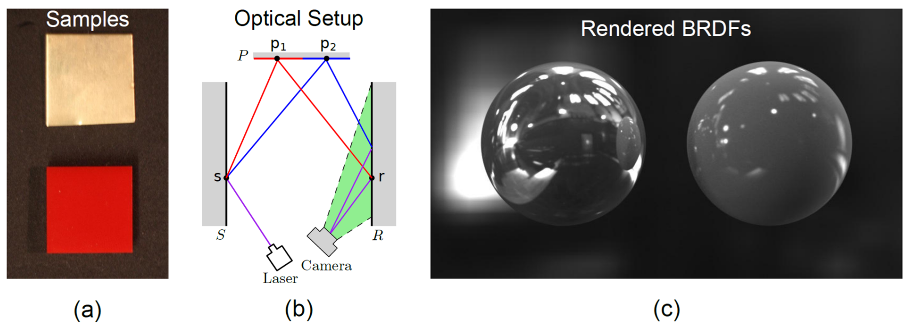

Figure 5. Acquiring parametric BRDFs. (a) Multiple material samples. (b) Indirect-imaging setup. (c) The recovered BRDFs match well with the data acquired with traditional methods.

Similarly to the "looking around corners" case, we acquire time-space streak images by focusing on a single line on the diffuser and illuminating it with pulsed laser on several locations. Using Eq. 1 we render synthetic streak images based on the scene geometry, where the only unknown is the albedo of scene points $(R(x'))$. We solve a nonlinear optimization problem for scene point albedos, that minimizes the error norm between the real streak images and the rendered streak images. We are able to accurately measure the albedo of several scene points in complex scenes (Fig. 4).

The Bidirectional Reflectance Distribution Function (BRDF) is a four-dimensional function that characterizes the relationship between the reflected and incident radiance for opaque surfaces. BRDFs are primarily used in the field of computer graphics for photorealistic rendering, image relighting, and material editing, as well as for matching and material identification. Traditional techniques in graphics directly illuminate and image a small sample of the material from various angles, to acquire material BRDFs (see[31] for a survey on acquisition techniques). Traditional BRDF acquisition methods are time consuming, need complex equipment encircling small material samples, and typically image only a single material at a time.

Ultrafast measurements enable us to tackle these challenges.[30] Unlike traditional techniques which rely on direct measurement of reflected light off the material surface, ToF measures all the bounces of light arriving at the diffuse surface, after interacting with material samples (Fig. 5). We acquire multiple streak images of indirect reflections from samples. The measurements and scene geometry are used in a linear system to solve for a low-dimensional parametric BRDF. We solve the linear system using unconstrained linear optimization, to recover BRDFs, which match well with BRDFs obtained with traditional methods, both in simulations and real experiments.

4. IMAGING AFTER CONTINUOUS SCATTERING

This section extends the previous imaging applications to cases in which there is significant time blur (due to fluorescence or volumetric scattering). Thus, the time dependency is not parameterized by a discrete function.

4.1 Recovering Fluorescence Lifetime Behind Scattering Layer

The ability to control and manipulate luminescent probes enables new capabilities in many imaging systems, such as high-resolution results in biological microscopy[32] and anti-fraud measures or covert tracking.[33] These applications can benefit from fluorescence lifetime imaging (FLI) measurement. While FLI requires more complex hardware, it provides information on the environment of the probes.[34,35] It also overcomes cases in which pure spectral signature is insufficient.[36] In particular, the extra information provided by FLI makes it attractive for imaging through complex media.

To demonstrate simultaneous recovery of location and fluorescence lifetime we consider again a reflection optical geometry (Fig. 2b).[37] The targets in this case are a set of three $1.5 \times 1.5 cm^2$ square patches hidden behind the diffuser. The first patch (NF) is non-fluorescent. The second patch (QD) is painted with a quantum dot solution ($\tau = 32ns, \lambda_{emission} \sim 652nm$). The third patch (PI) is painted with Pyranine ink ($\tau = 5ns, \lambda_{emission} \sim 510nm$).

In order to incorporate the fluorescence profile into our mathematical model, we assume a time-defendant reflectance profile with an exponential decay in Eq. 1:

$$R(x', t) = \rho(x')\tau^{-1}(x')e^{-t/\tau(x')}u(t) \tag{2}$$

where $\tau(x')$ is the local fluorescence lifetime, and $u(t)$ is a unit step function, imposed to satisfy causality.

The main challenge in the reconstruction process is the coupling between the geometrical information (high frequency data encoded in space and time) and fluorescence profile (low frequency data encoded in time). While previously the time profile encoded just geometry (as seen in Fig. 6a), now the geometrical features are not readily observable since they are masked by the fluorescence profile (Fig. 6b). Ideally we want to recover locations and lifetimes simultaneously. However the problem is ill-posed and the search space is too large. In order to overcome this challenge we first aim to recover a coarse location map of possible locations, followed by a step to recover both locations and lifetimes simultaneously. The first step narrows the search space of the second step, thus making the entire process robust.[38] To computationally solve these two steps we assume the patches are sparse in space and use orthogonal matching pursuit.[39] To demonstrate our method we show results for three different configurations in Table 1. We are able to correctly classify all patches, and recover their locations.

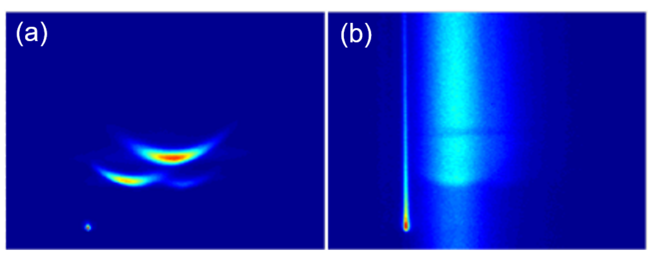

Figure 6. Fluorescing tags behind scattering layer. a) Streak measurement of the targets, due to strong direct reflection from the patches we observe only geometrical features and no fluorescence profile. b) Streak measurement taken with a UV filter to block the direct reflection reveals the fluorescence profile which obscures the pure geometrical data.

	Configuration 1				Configuration 2				Configuration 3			
Patch	ΔX	ΔY	ΔZ	Δτ	ΔX	ΔY	ΔZ	Δτ	ΔX	ΔY	ΔZ	Δτ
QD	8.1	9.9	1.6	0	5.8	14.6	1.67	0	4.8	7.0	2.6	0
PI	5.7	10.9	1.6	0	2.4	14.3	2.13	0	6.9	16.7	1.7	0

Table 1. Reconstruction error; the numbers represent distances from the center of each ground truth patch in space to the center of the corresponding reconstructed patch. Length units are millimeters.

4.2 Imaging Through Volumetric Scattering

Another case of ultrafast imaging with significant blurring in time occurs when the signal goes through volumetric scattering. While previous examples looked into cases of discrete scattering events (in the fluorescence case it is a discrete event overlaid by a continuous function), here we consider a case of continuous scattering that occurs when light propagates through thick biological tissue. Ultrafast measurement allows to overcome these challenges by measuring the imaging system's point spread function (PSF) in space as well as in time.[4]

Here, the optical setup is transmission mode (Fig. 2c), where we use the rotating mirrors to capture a complete measurement of the $x-y-t$ space. The first step in the reconstruction process is to measure the system's PSF. This is achieved by placing a pin hole mask behind the thick diffuser. The following forward model is empirically fit to the measurement:

$$PSF(x,y,t) = \frac{1}{t} exp\left(-\frac{(\ln t-\mu)^2}{2\sigma^2}\right) exp\left(-\frac{x^2+y^2}{4\,(D_0+D_1 t)}\right) \tag{3}$$

where μ, σ, D_0, D_1 are the model parameters. Fig. 7. shows the measured PSF and the fitted model.

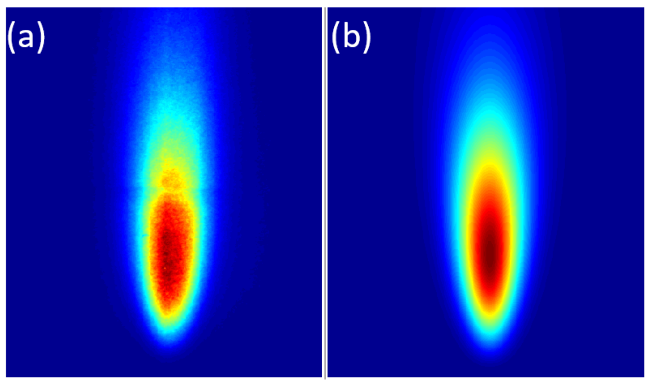

Figure 7. PSF estimation (a) Streak measurement of the PSF (showing a cross section for $y = 0$). (b) The corresponding cross section of our empirical PSF.

This forward model allows to cast the general problem of scene recovery as an optimization problem. The goal is to find a target which minimizes the difference between the $x-y-t$ measurement to a predicted measurement. We demonstrate our method and compare it to other techniques in Fig. 8.

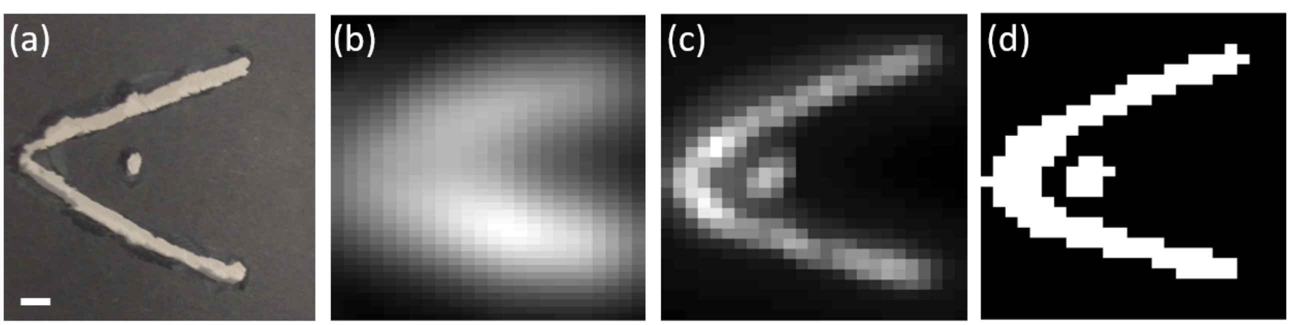

Figure 8. Imaging through volumetric scattering. (a) The mask hidden behind the diffuser (white scale bar: 4mm). (b) Result of imaging without using time-domain information. (c) Reconstruction using our algorithm. (d) Applying a threshold to generate a binary image from the reconstruction in panel (c).

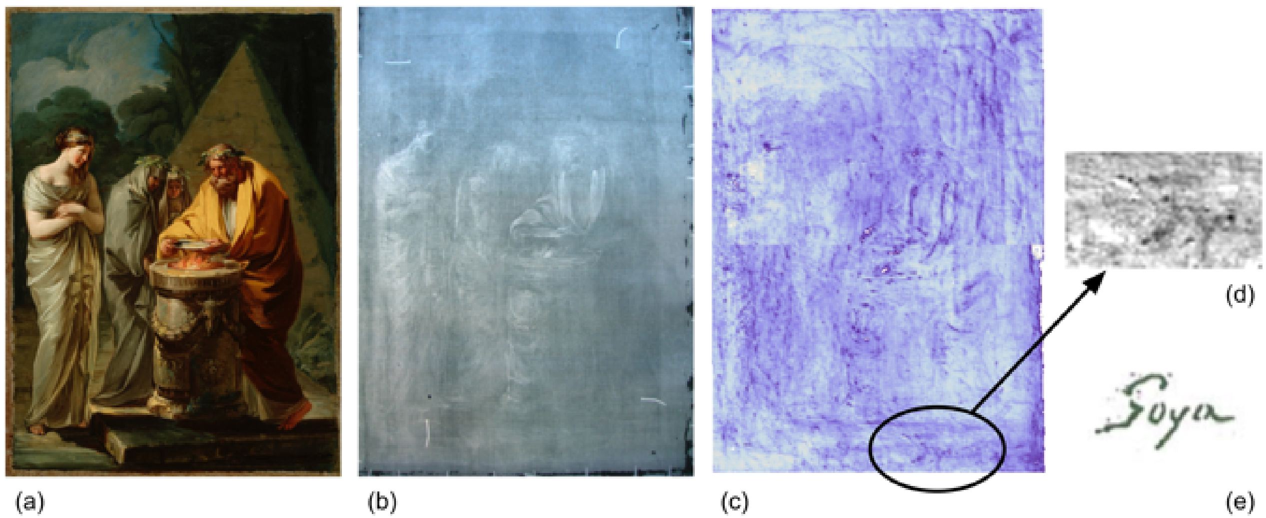

Figure 9. Results of inspecting Goya's "Sacrifice to Vesta" with Terahertz. (a) Painting in the optical range. (b) X-ray image of the same painting. (c) Terahertz amplitude image of a deep layer. (d) Zoom in area with a feature that resembles the signature of the artist. (e) Registered signature of the artist.

5. IMAGING LAYERED STRUCTURES WITH PULSED TERAHERTZ WAVES

All imaging methods described in the paper thus far make use of visible and near IR wavelengths. We now describe the use of Terahertz (THz) range of the electromagnetic spectrum, which spans the frequencies from 0.1 THz to 10 THz.[40,41] THz waves offer some unique features, such as the ability to penetrate dielectric materials and wavelengths short enough to resolve sub-mm spatial features (i.e., 1 THz is 300 um). THz time-domain comprises the methods and techniques to generate and detect sub-picosecond pulses in time. The frequency components of such picosecond pulses extend into the THz range and, therefore, they are also referred to as THz pulses or THz waves. THz time-domain technology is attractive for non-destructive testing (NDT) applications,[42,43] for example detecting structural defects in foam, wooden objects,[44] plastic components[45] and cultural artifacts.[46–48]

One particular field that benefits from the properties of time-domain THz is cultural heritage. For example, paintings comprise of different layers made of different materials, which may have different content. Current methods (visible, infrared, ultraviolet, and X-ray) are not able to retrieve the content of deep layers; underpaints or other features remain blocked by the top layers. THz waves are more sensitive to chemical composition and offer sub-millimeter resolution to resolve these small details. THz ToF data of the entire depth section of the painting makes them suitable to analyze the different layers of a painting. However, many challenges arise due to the thickness of layers and gaps which are comparable to the wavelength of the THz pulse. For example, the SNR degrades very quickly as the number of layers increases, the contrast of the content in each layer is low and comparable to the contrast from inter-reflection noise, and, content from one layer occludes and causes shadowing effects in the signals coming from deeper layers. We tackle these challenges with computational approaches. The result allow us to retrieve the content of each different layer in the sample.

Fig. 9 shows the results of using THz to unravel the signature of master Goya in his early painting "Sacrifice to Vesta", 1771 (Fig. 9a). The signature is not visible in the optical nor in the infrared or ultraviolet domain, since is it blocked by a thick layer of lacquer that becomes dark over time. X-ray image (Fig. 9b) shows areas with a high content of lead-based paint, and the nails and frame, but fails to catch subtle features. The THz image (Fig. 9c) is able to capture texture of brush strokes and other structural features that indicate stress in the canvas. However, the most interesting feature is captured in the lower right part of the painting. This feature (Fig. 9d) resembles the signature of the painter (Fig. 9e) and, thus, provides evidence of the authenticity of the piece.[49]

6. NOVEL IMAGING ARCHITECTURES

While ultrafast imaging has been widely used to image through scattering barriers, new studies suggest that it can be used to change the imaging interface itself. Currently most of imaging systems are lens-based systems that are suitable for imaging through air or other transparent media. However, when imaging and sensing through complex harsh environments (e.g. porous media, diffusive liquids, high temperature and pressure, etc.) and complex geometries (geometries proper for endoscopy), fiber-based imaging can be a better imaging interface. Conventionally fiber-based image guides such as coherent fiber bundles have been used for such conditions. In longer length, however, (more than $20cm$) coherent fiber bundles are rather rigid and fragile and they cannot provide wide field of view. We use ToF to enable imaging through randomly distributed and permuted sets of fibers.[50] This imaging interface (named optical brush) provides a brush-like flexible form factor.

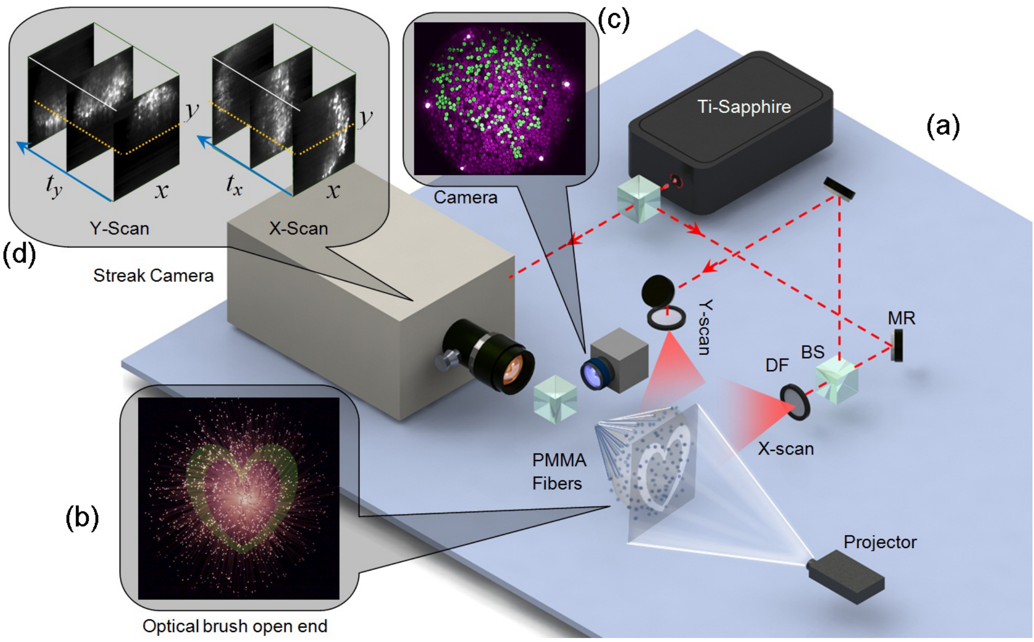

Figure 10. Setup for an optical brush enabled with ultrafast imaging. (a) Setup consists of a streak camera triggered by Ti-Sapphire pulses and an ordinary camera placed on the closed end of the optical brush. The other end is fed with a synthetic scene via a projector. BS stands for beam splitter and DF stands for diffuser. (b) Front view of the open-end of the optical brush with image of the heart projected on to the fibers. The infrared pulses are propagating in off-axis (perpendicular) with the plane that the fibers are distributed in. (c) Shuffled output of the brush seen by an ordinary camera. (d) Streak camera output. Each x-t slice is a streak image.

The optical brush uses a pulsed ToF technique for non-coaxial calibration of randomly distributed fibers to reconstruct the image of a scene for a secondary camera. Fig. 10a shows the setup for an optical brush: the fibers bristles are scanned with pulsed planar wavefronts. A projector is used to make a synthetic 2D scene for the brush (Fig. 10b). Since the fibers are randomly distributed in the 2D scene plane, the camera sees a lossy permuted or "shuffled" image of the scene as in Fig. 10c.

The streak measurements allow us to map between input and output positions of the fibers to reconstruct the target. This map is based on the time in which the pulse is received in the streak image for each fiber. This time correlates directly to the position of that fiber at the open-end. For instance, since all the fibers are equal in length, a fiber that outputs the pulsed signal later in time by the sweeping X-scan pulse (propagating from right to left) should be also positioned further away to the left.

Fig. 11a show an example of an input scene that is fed into the optical brush. As seen in Fig. 11b, the input is completely shuffled and some of the pixels are lost. Fig. 11c shows the deshuffled result by ToF technique. Fig. 11d shows ToF results superimposed on top of a lower resolution reference obtained by raster scanning the fibers (cyan color). The ToF technique provides a 400×400 lateral resolution $(X - Y)$ based on the time resolution of streak data cubes.

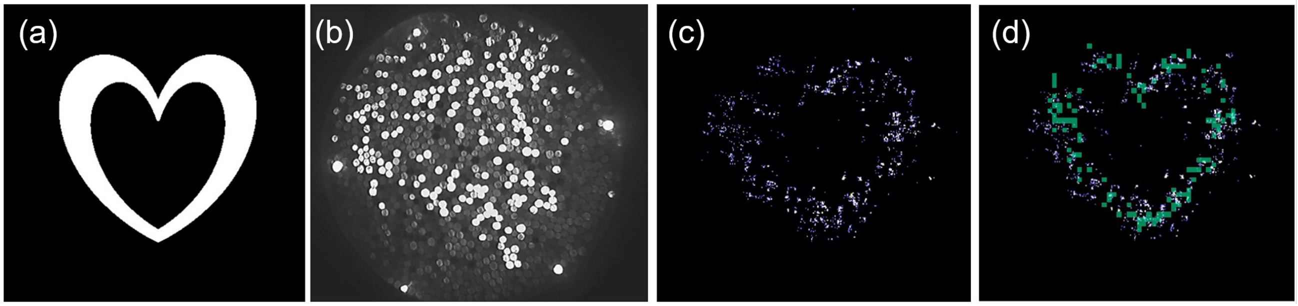

Figure 11. Ultrafast imaging used to reorganize pixels in imaging with and optical brush. (a) Input image. (b) Shuffled image that is output from the brush. (c) Deshuffled image based on off-axis ToF deshuffling technique. The spots are weighed based on the original intensity of the fibers in the streak data cubepoints with higher intensity represent fibers with brighter IR output from the sweeping pulses. (d) Deshuffled (400×400) image is superimposed on coaxial raster scan reference $(60 \times 80$ resolution) for comparison.

Instead of using ToF to reveal 3D depth information, an optical brush uses this parameter to change the physical form of the imaging or sensing interface for a second camera. This enabling perspective on ToF parameter can be combined with emerging and preexisting ToF techniques such as continuous wave ToF,[9,51,52] sequentially time all-optical mapping,[53] coherent interferometric depth imaging techniques[54,55] and pulsed ToF methods.[1] Such change in physical form can affect acquisition capability with applications in biomedical imaging,[56] photophysics,[19] and industrial sensing.[1] The ToF enabled optical brush, therefore, has significant potential for endoscopy, imaging in turbid media[23,57,58] and near-field batch probing.[59]

7. FUTURE SENSORS AND SOURCES

Conventionally, single-photon avalanche diodes (SPADs) have been one of the key players for applications that required high sensitivity. While streak cameras are making steady progress in their time resolution, with the introduction of Time-Correlated Single-Photon Counting (TCSPC) and improvement in circuit architecture, time-sensitive SPAD cameras are now entering the realm of ToF applications.[60] One of the most promising directions is incorporation of these cameras for biomedical imaging. However, while the sensitivity of SPADs promises imaging through thick pieces of living tissue, the time resolution and spatial resolution are still a burden. Fig. 12 demonstrates the advantage of single-photon sensitivity when encountering a thick tissue sample.

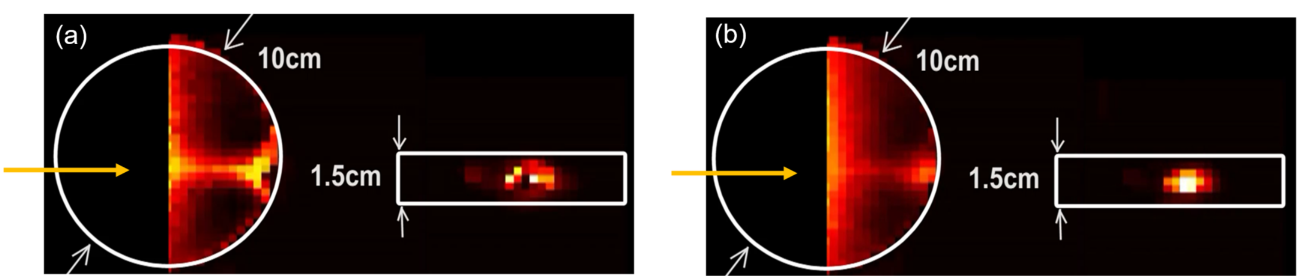

Figure 12. IR pulse ($20mW/cm^2$, $790nm$, $50fs$) passing through $10cm$ of tissue phantom disk. (a),(b) showing different time frames separated by $1.3ns$. Half of the phantom is covered to avoid camera saturation. Pixels at the center of the bright region are black due to saturation. The orange arrow shows the direction of pulse propagation. There is an exponential decay in the pulse intensity as it travels through the sample; this along with strong scattering at the phantom-air interface required us to block the left half of the phantom disk to investigate the other half.

As the sensitivity of pulsed-mode ToF sensors is increasing, the need for higher power laser sources is now decreasing, enabling lower cost longer pulse width lasers to be used in ultrafast imaging systems.[61] On the other side of the spectrum as the electronics speed is increasing, continuous wave ToF cameras are starting to be applied in some of the ultrafast imaging applications such as high resolution depth sensing[62] and fluorescent lifetime imaging.[51] However, both continuous wave cameras and SPADs are fundamentally incapable of providing single shot ultrafast information as they depend on periodicity of acquisition. Therefore, unlike streak cameras these new technologies are not suitable for study of irreversible phenomena.[18, 19]

8. CONCLUSIONS

We presented how ultrafast detectors and sources enable non-line of sight imaging, which results in novel imaging applications. Different detection solutions provide a wide range of trade-offs, for example SPAD provides great sensitivity and a 2D array but doesn't allow a single shot acquisition and currently has limited time resolution. We also demonstrated non-traditional acquisition modality in the form of an optical brush as well as emerging opportunities in the THz spectrum. Various non-line of sight applications are enabled by ultrafast measurement, such as recovering material properties (albedo, fluorescence lifetime) behind scattering layers.

REFERENCES

[1] Velten, A., Willwacher, T., Gupta, O., Veeraraghavan, A., Bawendi, M. G., and Raskar, R., "Recovering three-dimensional shape around a corner using ultrafast time-of-flight imaging," *Nature communications* **3**, 745 (jan 2012).

[2] Naik, N., Barsi, C., Velten, A., and Raskar, R., "Estimating wide-angle, spatially varying reflectance using time-resolved inversion of backscattered light," *Journal of the Optical Society of America. A, Optics, image science, and vision* **31**, 957–963 (may 2014).

[3] Satat, G., Heshmat, B., Barsi, C., Raviv, D., Chen, O., Bawendi, M. G., and Raskar, R., "Locating and classifying fluorescent tags behind turbid layers using time-resolved inversion," *Nature Communications* **6** (2015).

[4] Satat, G., Raviv, D., Heshmat, B., and Raskar, R., "Imaging through thick turbid medium using time-resolved measurement," in [*Computational Optical Sensing and Imaging*], CT3F–4, Optical Society of America (2015).

[5] Raviv, D., Barsi, C., Naik, N., Feigin, M., and Raskar, R., "Pose estimation using time-resolved inversion of diffuse light," *Optics Express* **22**, 20164 (aug 2014).

[6] Huang, D., Swanson, E., Lin, C., Schuman, J., Stinson, W., Chang, W., Hee, M., Flotte, T., Gregory, K., Puliafito, C., and Et, A., "Optical coherence tomography," *Science* **254**, 1178–1181 (nov 1991).

[7] Satat, G., Barsi, C., and Raskar, R., "Skin perfusion photography," in [*2014 IEEE International Conference on Computational Photography (ICCP)*], 1–8, IEEE (may 2014).

[8] Ng, R., Levoy, M., Brédif, M., Duval, G., Horowitz, M., and Hanrahan, P., "Light field photography with a hand-held plenoptic camera," Tech. Rep. 11 (2005).

[9] Kadambi, A., Taamazyan, V., Shi, B., and Raskar, R., "Polarized 3D: High-Quality Depth Sensing With Polarization Cues," in [*Proceedings of the IEEE International Conference on Computer Vision*], 3370–3378 (2015).

[10] Adelson, E. H. and Bergen, J. R., [*The plenoptic function and the elements of early vision*], Vision and Modeling Group, Media Laboratory, Massachusetts Institute of Technology (1991).

[11] Seitz, S., Matsushita, Y., and Kutulakos, K., "A theory of inverse light transport," in [*Tenth IEEE International Conference on Computer Vision (ICCV'05) Volume 1*], **2**, 1440–1447 Vol. 2, IEEE (2005).

[12] Kajiya, J. T., "The rendering equation," *ACM SIGGRAPH Computer Graphics* **20**, 143–150 (aug 1986).

[13] Ramesh, R. and Davis, J., "5d time-light transport matrix: What can we reason about scene properties?," (mar 2008).

[14] Wu, D., Wetzstein, G., Barsi, C., Willwacher, T., O'Toole, M., Naik, N., Dai, Q., Kutulakos, K., and Raskar, R., [*Computer Vision – ECCV 2012: 12th European Conference on Computer Vision, Florence, Italy, October 7-13, 2012, Proceedings, Part I*], ch. Frequency Analysis of Transient Light Transport with Applications in Bare Sensor Imaging, 542–555, Springer Berlin Heidelberg, Berlin, Heidelberg (2012).

[15] Ranka, J. K., Gaeta, A. L., Baltuska, A., Pshenichnikov, M. S., and Wiersma, D. A., "Autocorrelation measurement of 6-fs pulses based on the two-photon-induced photocurrent in a GaAsP photodiode," *Optics Letters* **22**, 1344 (sep 1997).

[16] Heshmat, B., Pahlevaninezhad, H., and Darcie, T., "Efficient low-power autocorrelation measurement with carbon nanotube photoconductors," in [*Conference on Lasers and Electro-Optics 2012*], JW2A.3, OSA, Washington, D.C. (may 2012).

[17] Nabekawa, Y., Shimizu, T., Okino, T., Furusawa, K., Hasegawa, H., Yamanouchi, K., and Midorikawa, K., "Interferometric autocorrelation of an attosecond pulse train in the single-cycle regime.," *Physical review letters* **97**, 153904 (oct 2006).

[18] Heshmat, B., Satat, G., Barsi, C., and Raskar, R., "Single-shot ultrafast imaging using parallax-free alignment with a tilted lenslet array," *Cleo: 2014* **1**(1), STu3E.7 (2014).

[19] Gao, L., Liang, J., Li, C., and Wang, L. V., "Single-shot compressed ultrafast photography at one hundred billion frames per second," *Nature* **516**, 74–77 (dec 2014).

[20] Velten, A., Raskar, R., Wu, D., Jarabo, A., Masia, B., Barsi, C., Joshi, C., Lawson, E., Bawendi, M., and Gutierrez, D., "Femto-photography," *ACM Transactions on Graphics* **32**, 1 (jul 2013).

[21] Sen, P., Chen, B., Garg, G., Marschner, S. R., Horowitz, M., Levoy, M., and Lensch, H. P. A., "Dual photography," *ACM Transactions on Graphics* **24**, 745–755 (jul 2005).

[22] Ariese, F., Meuzelaar, H., Kerssens, M. M., Buijs, J. B., and Gooijer, C., "Picosecond Raman spectroscopy with a fast intensified CCD camera for depth analysis of diffusely scattering media.," *The Analyst* **134**, 1192–7 (jun 2009).

[23] Wu, J., Wang, Y., Perelman, L., Itzkan, I., Dasari, R. R., and Feld, M. S., "Three-dimensional imaging of objects embedded in turbid media with fluorescence and Raman spectroscopy.," *Applied optics* **34**, 3425–30 (jun 1995).

[24] Takahashi, E., Kato, S., Furutani, H., Sasaki, A., Kishimoto, Y., Takada, K., Matsumura, S., and Sasaki, H., "Single-shot observation of growing streamers using an ultrafast camera," *Journal of Physics D: Applied Physics* **44**, 302001 (aug 2011).

[25] Heshmat, B., Pahlevaninezhad, H., and Darcie, T. E., "Carbon Nanotube-Based Photoconductive Switches for THz Detection: An Assessment of Capabilities and Limitations," *IEEE Photonics Journal* **4**, 970–985 (jun 2012).

[26] Ibrahim, A., Férachou, D., Sharma, G., Singh, K., Kirouac-Turmel, M., and Ozaki, T., "Ultra-high dynamic range electro-optic sampling for detecting millimeter and sub-millimeter radiation," *Scientific Reports* **6**, 23107 (mar 2016).

[27] Heshmat, B., Masnadi-Shirazi, M., Lewis, R. B., Zhang, J., Tiedje, T., Gordon, R., and Darcie, T. E., "Enhanced Terahertz Bandwidth and Power from GaAsBi-based Sources," *Advanced Optical Materials* **1**, 714–719 (oct 2013).

[28] Gupta, O., Willwacher, T., Velten, A., Veeraraghavan, A., and Raskar, R., "Reconstruction of hidden 3D shapes using diffuse reflections.," *Optics express* **20**, 19096–108 (aug 2012).

[29] Naik, N., *Multibounce light transport analysis using ultrafast imaging for material acquisition*, PhD thesis, Massachusetts Institute of Technology (2012).

[30] Naik, N., Zhao, S., Velten, A., Raskar, R., and Bala, K., "Single view reflectance capture using multiplexed scattering and time-of-flight imaging," in [*ACM Transactions on Graphics (TOG)*], **30**(6), 171, ACM (2011).

[31] Weyrich, T., Lawrence, J., Lensch, H., Rusinkiewicz, S., and Zickler, T., "Principles of appearance acquisition and representation," *Foundations and Trends® in Computer Graphics and Vision* **4**(2), 75–191 (2009).

[32] Lichtman, J. W. and Conchello, J.-A., "Fluorescence microscopy," *Nature methods* **2**, 910–919 (dec 2005).

[33] Williams, Jr., G. M., Allen, T., Dupuy, C., Novet, T., and Schut, D., "Optically coded nanocrystal taggants and optical frequency IDs," in [*SPIE Defense, Security, and Sensing*], 76730M, International Society for Optics and Photonics (apr 2010).

[34] Lackowicz, J. R., [*Principles of Fluorescence Spectroscopy*], Springer (2006).

[35] Redford, G. I., Majumdar, Z. K., Sutin, J. D. B., and Clegg, R. M., "Properties of microfluidic turbulent mixing revealed by fluorescence lifetime imaging," *The Journal of chemical physics* **123**, 224504 (dec 2005).

[36] Koenig, K., Wollina, U., Riemann, I., Peukert, C., Halbhuber, K.-J., Konrad, H., Fischer, P., Fuenfstueck, V., Fischer, T. W., and Elsner, P., "Optical tomography of human skin with subcellular spatial and picosecond time resolution using intense near infrared femtosecond laser pulses," in [*International Symposium on Biomedical Optics*], 191–201, International Society for Optics and Photonics (jun 2002).

[37] Satat, G., Barsi, C., Heshmat, B., Raviv, D., and Raskar, R., "Locating fluorescence lifetimes behind turbid layers non-invasively using sparse, time-resolved inversion," in [*CLEO: QELS_Fundamental Science*], JTh2A–43, Optical Society of America (2014).

[38] Satat, G., *Imaging through scattering*, PhD thesis, Massachusetts Institute of Technology (2015).

[39] Pati, Y., Rezaiifar, R., and Krishnaprasad, P., "Orthogonal matching pursuit: recursive function approximation with applications to wavelet decomposition," in [*Proceedings of 27th Asilomar Conference on Signals, Systems and Computers*], 40–44, IEEE Comput. Soc. Press (1993).

[40] Tonouchi, M., "Cutting-edge terahertz technology," *Nat. Photonics.* **1**(2), 97–105 (2007).

[41] Siegel, P. H., "Terahertz technology," *IEEE Trans. Microw. Theory Techn.* **50**, 910–928 (Mar. 2002).

[42] Jansen, C., Wietzke, S., Peters, O., Scheller, M., Vieweg, N., Salih, M., Krumbholz, N., Joerdens, C., Hochrein, T., and Koch, M., "Terahertz imaging: applications and perspectives," *Appl. Opt.* **49**(19), E48–E57 (2010).

[43] Horiuchi, N., "Terahertz technology: Endless applications," *Nat. Photonics.* **4**, 140–140 (Mar. 2010).

[44] Jördens, C., Wietzke, S., Scheller, M., and Koch, M., "Investigation of the water absorption in polyamide and wood plastic composite by terahertz time-domain spectroscopy," *Polym. Test.* **29**, 209–215 (Apr. 2010).

[45] Wietzke, S., Jördens, C., Krumbholz, N., Baudrit, B., Bastian, M., and Koch, M., "Terahertz imaging: a new non-destructive technique for the quality control of plastic weld joints," *J. Eur. Opt. Soc. Rapid* **2** (Apr. 2007).

[46] Jackson, B., Bowen, J. W., and Walker, G. C., "A survey of terahertz applications in cultural heritage conservation science," *IEEE Trans. THz Sci. Technol.* **1**, 220–231 (Sept. 2011).

[47] Fukunaga, K. and Hosako, I., "Innovative non-invasive analysis techniques for cultural heritage using terahertz technology," *C. R. Phys.* **11**, 519–526 (Aug. 2010).

[48] Manceau, J.-M., Nevin, A., Fotakis, C., and Tzortzakis, S., "Terahertz time domain spectroscopy for the analysis of cultural heritage related materials," *Appl. Phys. B* **90**, 365–368 (Mar. 2008).

[49] Seco-Martorell, C., López-Domínguez, V., Arauz-Garofalo, G., Redo-Sanchez, A., and Tejada, J., "Goya's artwork imaging with Terahertz waves," *Opt. Express* **21**, 17800–17805 (July 2013).

[50] Heshmat, B., Lee, I. H., and Raskar, R., "Optical brush: Imaging through permuted probes," *Scientific Reports* **6**, 20217 (feb 2016).

[51] Bhandari, A., Barsi, C., and Raskar, R., "Blind and reference-free fluorescence lifetime estimation via consumer time-of-flight sensors," *Optica* **2**, 965 (nov 2015).

[52] Naik, N., Kadambi, A., Rhemann, C., Izadi, S., Raskar, R., and Bing Kang, S., "A light transport model for mitigating multipath interference in time-of-flight sensors," 73–81 (2015).

[53] Nakagawa, K., Iwasaki, A., Oishi, Y., Horisaki, R., Tsukamoto, A., Nakamura, A., Hirosawa, K., Liao, H., Ushida, T., Goda, K., Kannari, F., and Sakuma, I., "Sequentially timed all-optical mapping photography (STAMP)," *Nature Photonics* **8**, 695–700 (aug 2014).

[54] Cižmár, T. and Dholakia, K., "Exploiting multimode waveguides for pure fibre-based imaging.," *Nature communications* **3**, 1027 (jan 2012).

[55] Adler, D. C., Chen, Y., Huber, R., Schmitt, J., Connolly, J., and Fujimoto, J. G., "Three-dimensional endomicroscopy using optical coherence tomography," *Nature Photonics* **1**, 709–716 (nov 2007).

[56] Goda, K., Tsia, K. K., and Jalali, B., "Serial time-encoded amplified imaging for real-time observation of fast dynamic phenomena.," *Nature* **458**, 1145–9 (apr 2009).

[57] Patwardhan, S. V. and Culver, J. P., "Quantitative diffuse optical tomography for small animals using an ultrafast gated image intensifier," *Journal of biomedical optics* **13**(1), 011009–011009 (2008).

[58] Flusberg, B. A., Cocker, E. D., Piyawattanametha, W., Jung, J. C., Cheung, E. L. M., and Schnitzer, M. J., "Fiber-optic fluorescence imaging.," *Nature methods* **2**, 941–950 (2005).

[59] Chibani, H., Dukenbayev, K., Mensi, M., Sekatskii, S. K., and Dietler, G., "Near-field scanning optical microscopy using polymethylmethacrylate optical fiber probes.," *Ultramicroscopy* **110**, 211–5 (feb 2010).

[60] Gariepy, G., Krstajić, N., Henderson, R., Li, C., Thomson, R. R., Buller, G. S., Heshmat, B., Raskar, R., Leach, J., and Faccio, D., "Single-photon sensitive light-in-fight imaging.," *Nature communications* **6**, 6021 (jan 2015).

[61] Squier, J. and Muller, M., "High resolution nonlinear microscopy: A review of sources and methods for achieving optimal imaging," *Review of Scientific Instruments* **72**, 2855 (jul 2001).

[62] Kadambi, A., Whyte, R., Bhandari, A., Streeter, L., Barsi, C., Dorrington, A., and Raskar, R., "Coded time of flight cameras," *ACM Transactions on Graphics* **32**, 1–10 (nov 2013).